CCS CHINESE CHEMICAL SOCIETY   PEKING UNIVERSITY 1898   ROYAL SOCIETY OF CHEMISTRY

RESEARCH ARTICLE

Check for updates

Gold(III)-mediated insertion of Se and Te into Au–P bonds: *en route* to diphosphane chalcogenides and σ-hole modulation

Juan Carlos Pérez-Sánchez, [ID] [a,b] Jesús Moradell, [ID] [a] Juan V. Alegre-Requena, [ID] [a] Raquel P. Herrera [ID] [b] and M. Concepción Gimeno [ID] *[b]

We report an unprecedented gold(III)-templated insertion of selenium and tellurium into Au–P bonds of bis(diphenylphosphane)methane (dppm), affording the first examples of κ^2E,P Au(III) metallacycles (E = Se, Te) *via* direct chalcogen transfer under mild conditions. This transformation represents a rare case of heavy-chalcogen incorporation into a metal–phosphorus bond, providing synthetic access to previously elusive Te-functional diphosphanes and extending to their selenium congeners. Structural, spectroscopic, and computational analyses reveal that Au coordination modulates P–E covalency and charge distribution, yielding electronically diverse chalcogenated frameworks. Beyond synthetic novelty, these Au–E–P scaffolds act as potent chalcogen-bond (ChB) donors in transfer hydrogenation, with Te complexes outperforming their Se analogues in line with deeper, more accessible Te σ-holes. Remarkably, their catalytic efficiency parallels that of metal-free phosphonium chalcogenides, prepared by direct methylation of $(^iPr)_3P{=}E$ for comparative evaluation. The synergy between Au coordination and chalcogen identity facilitates direct access to otherwise inaccessible Te-functional diphosphanes and establishes a modular platform for tuning σ-hole interactions, advancing the design of main-group/transition-metal hybrids for noncovalent catalysis and molecular materials.

Introduction

Insertion reactions represent a powerful strategy in coordination and organometallic chemistry, enabling a wide range of transformations from hydrofunctionalisation to migratory insertion.[1] While extensively developed for small unsaturated molecules, such as CO, alkenes, or alkynes,[2] the formal insertion of group 16 elements into metal–ligand bonds remains a rare and mechanistically fascinating event.[3] In particular, the selective incorporation of heavier chalcogens such as selenium and tellurium into metal–phosphorus frameworks represents an underdeveloped area with broad implications for ligand design, electronic modulation, and the generation of heteroatom-functionalised diphosphanes. Phosphane chalcogenides ($R_3P{=}E$, E = S, Se, Te) are valuable reagents owing to their tuneable donor strength, redox activity, and stereoelectronic properties.[4] Yet, their engagement in metal-centred bond acti-

vation pathways remains poorly understood. Typically, these species coordinate to metals *via* donor–acceptor interactions, while direct chalcogen insertion into M–P bonds has scarcely been documented. This limitation is particularly striking for tellurium, whose low bond dissociation energy and high polarisability hinder predictable bonding and reactivity.[4c] This challenge is particularly pronounced for the telluration of aromatic phosphanes, such as those containing Ph_2P moieties, which exhibit significantly limited reactivity toward tellurium, rendering direct telluration of diphosphanes like dppm (1,1′-bis(diphenylphosphane)methane) synthetically inaccessible (Scheme 1a).[5] To date, stable Te-containing diphosphanes have been largely restricted to electron-rich scaffolds, such as anionic PNP or PCP-type ligands, and their reactivity toward coinage metals has scarcely been explored. In this context, recent studies have unveiled redox non-innocent behaviour in PNP phosphane tellurides upon coordination to d^{10} metals (Au^I and Ga^{III}), involving formal metal insertion into P–Te bonds coupled to two-electron redox events and P(V) → P(III) reduction (Scheme 1b).[6] Complementary routes based on metathesis or stepwise oxidation of PCP/PNP frameworks have produced monotellurido diphosphane complexes (Scheme 1c),[7,8] while the mono- and dichalcogenation of R_2PZPR_2 compounds (Z = $(CH_2)_n$, NH, CH and R = alkyl or

[a]Department of Inorganic Chemistry, Instituto de Síntesis Química y Catálisis Homogénea (ISQCH), CSIC-Universidad de Zaragoza, C/ Pedro Cerbuna 12, 50009 Zaragoza, Spain. E-mail: gimeno@unizar.es
[b]Department of Organic Chemistry, Laboratorio de Organocatálisis Asimétrica, Instituto de Síntesis Química y Catálisis Homogénea (ISQCH), CSIC-Universidad de Zaragoza, C/ Pedro Cerbuna 12, 50009 Zaragoza, Spain
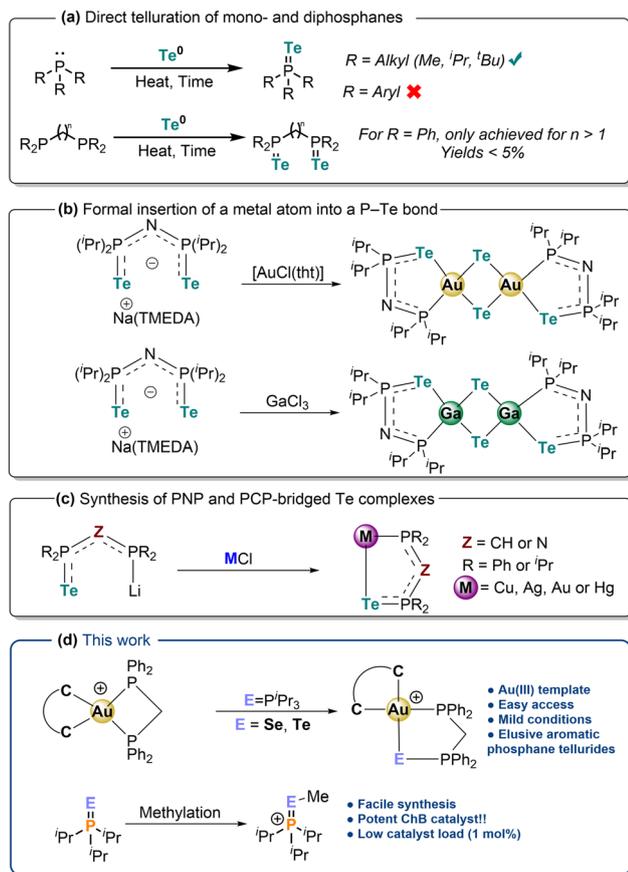
Scheme 1 (a–c) Previous examples of phosphane telluride metal complexes and formal insertion reactions. (d) Heavy chalcogen insertion into a P–Au bond and phosphonium chalcogenides described in this work.

aryl) has long been established and is high yielding.[9] Chivers and co-workers reported the PCP-bridged monochalcogenides $EP^iPr_2CH_2P^iPr_2$ (E = Te, Se). The tellurium derivative displays rapid intermolecular Te exchange in solution, as evidenced by NMR experiments and supported by DFT calculations, whereas the selenium analogue undergoes exchange at a significantly slower rate. The marked lability of the P–Te bond highlights the dynamic nature of these ligands and underscores their potential utility in coordination chemistry.[9b] However, related reactions involving elemental tellurium remain largely unexplored, and only a limited number of coinage–metal complexes featuring M–TePR₃ motifs (M = Cu, Ag, Au) have been described.[6b,8b,10,11]

Herein, we report a new and conceptually distinct transformation, the selective insertion of a heavy chalcogen (E = Se or Te) into a gold(III)–phosphorus bond. Remarkably, this transformation occurs exclusively with the heavier chalcogens, selenium and tellurium, and has no precedent for lighter analogues. This process expands the scope of metal–ligand bond activation to the heaviest chalcogens, offering a unique synthetic route to dppm-derived phosphane chalcogenides that cannot be obtained through direct oxidation with the elemental chalcogen, particularly in the case of tellurium

(Scheme 1d). Beyond its synthetic novelty, this transformation underscores the ability of late-transition-metal centres to mediate main-group element transfer and open new redox pathways relevant to the development of functional phosphane chalcogenides for catalysis, photonics, and molecular electronics. Moreover, the catalytic behaviour of these compounds has been evaluated and found to be comparable to that of the formal phosphonium chalcogenide analogues.
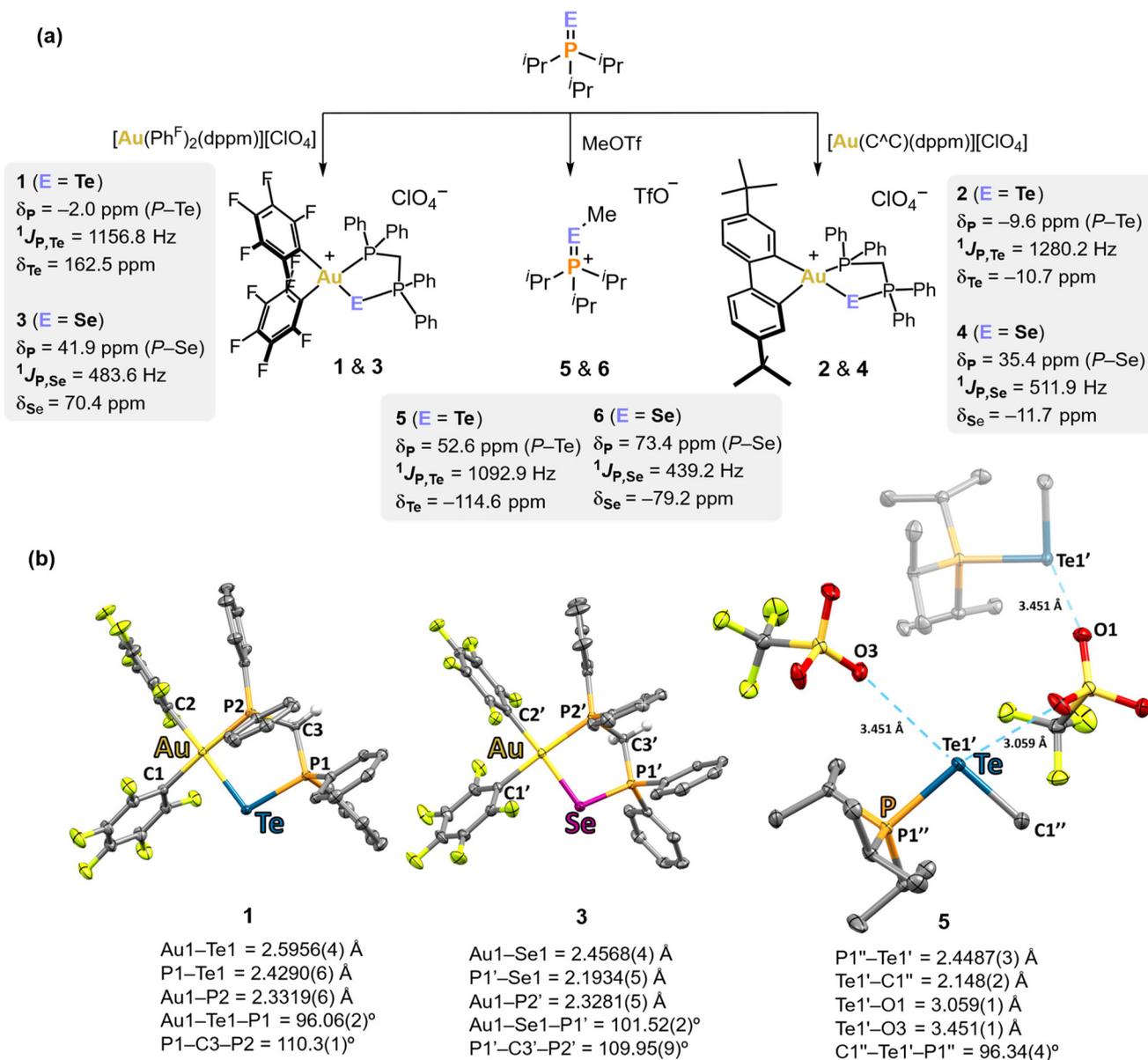
Results and discussion

Synthesis and characterisation of gold(III) complexes and phosphonium chalcogenides

Reacting either $[Au(C_6F_5)_2(dppm)][ClO_4]$[12] or $[Au(C^\wedge C)(dppm)][ClO_4]$[13] ($C^\wedge C$ = 4,4'-di-*tert*-butyl-1,1'-biphenyl) with one equivalent of $(^iPr)_3PTe$ at room temperature for 1 h yielded complexes **1** and **2**, respectively (Scheme 2). In the $^{31}P\{^1H\}$ NMR spectra, **1** displays two doublets at δ_P = 30.6 and −2.0 ppm (Fig. S2) and **2** at δ_P = 35.8 and −9.6 ppm (Fig. S6); the corresponding ^{125}Te resonances shift from δ_{Te} = +162.5 ppm (Fig. S4) to δ_{Te} = −10.7 ppm (Fig. S7) for **1** and **2**, respectively, consistent with minor back-donation from gold (III) at Te when using a stronger *trans*, more electron-rich $C^\wedge C$ ligand.[14] Furthermore, the $^1J(^{31}P,^{125}Te)$ signal is around 1200 Hz for both **1** and **2**, well below typical $J(P^V–Te)$ values (1650–2290 Hz),[4b,15] in line with P–Te lengthening upon Au coordination.[6b] To evaluate the generality of the insertion process and explore the effect of the chalcogen on the electronic properties of the resulting metallacycles, we extended our study from tellurium to selenium. Treatment of $[Au(C_6F_5)_2(dppm)]^+$ with $(^iPr)_3PSe$ at room temperature led to clean formation of complex **3**, under similar conditions to those used for tellurium. However, in contrast to the facile formation of the tellurium analogue **2**, the reaction of $(^iPr)_3PSe$ with the cyclometallated $[Au(C^\wedge C)(dppm)]^+$ required gentle heating to promote clean insertion and obtain complex **4**. The more forcing conditions required to access **4** relative to **3** can be rationalised by a combination of electronic and steric effects. In **4**, the cyclometallated $C^\wedge C$ ligand renders the Au(III) centre less electrophilic than in **3**, which bears strongly electron-withdrawing perfluorophenyl groups. As a consequence, activation of the coordinated phosphane selenide is attenuated, disfavoring the key intramolecular P–Se bond-forming step in which the pendant PPh₂ arm of dppm attacks the Au-bound $(^iPr)_3PSe$ fragment. In addition, increased steric congestion around the metal centre, arising from repulsive interactions between the *tert*-butyl substituents of the cyclometallated ligand and the phenyl groups of dppm, is expected to raise the barrier for the necessary bond reorganisation and chalcogen transfer. Consistent with the presence of a genuine kinetic barrier rather than simple time dependence, prolonged reaction times at room temperature did not lead to significant formation of **4**.

No reaction was observed when using lighter chalcogen analogues such as $(^iPr)_3P{=}S$ or $(^iPr)_3P{=}O$, even after extended

(a)

1 (E = Te)
δ_P = −2.0 ppm (P–Te)
$^1J_{P,Te}$ = 1156.8 Hz
δ_{Te} = 162.5 ppm

3 (E = Se)
δ_P = 41.9 ppm (P–Se)
$^1J_{P,Se}$ = 483.6 Hz
δ_{Se} = 70.4 ppm

2 (E = Te)
δ_P = −9.6 ppm (P–Te)
$^1J_{P,Te}$ = 1280.2 Hz
δ_{Te} = −10.7 ppm

4 (E = Se)
δ_P = 35.4 ppm (P–Se)
$^1J_{P,Se}$ = 511.9 Hz
δ_{Se} = −11.7 ppm

5 (E = Te)
δ_P = 52.6 ppm (P–Te)
$^1J_{P,Te}$ = 1092.9 Hz
δ_{Te} = −114.6 ppm

6 (E = Se)
δ_P = 73.4 ppm (P–Se)
$^1J_{P,Se}$ = 439.2 Hz
δ_{Se} = −79.2 ppm

(b)

1
Au1–Te1 = 2.5956(4) Å
P1–Te1 = 2.4290(6) Å
Au1–P2 = 2.3319(6) Å
Au1–Te1–P1 = 96.06(2)°
P1–C3–P2 = 110.3(1)°

3
Au1–Se1 = 2.4568(4) Å
P1'–Se1 = 2.1934(5) Å
Au1–P2' = 2.3281(5) Å
Au1–Se1–P1' = 101.52(2)°
P1'–C3'–P2' = 109.95(9)°

5
P1"–Te1' = 2.4487(3) Å
Te1'–C1" = 2.148(2) Å
Te1'–O1 = 3.059(1) Å
Te1'–O3 = 3.451(1) Å
C1"–Te1'–P1" = 96.34(4)°

Scheme 2 (a) Synthesis of compounds **1–6** from (^{i}Pr)$_3$P=E (E = Te or Se) and selected spectroscopic data (^{31}P{^{1}H}, ^{125}Te and ^{77}Se chemical shifts and $^1J_{P,E}$). Ph^F = pentafluorophenyl (C$_6$F$_5$); C^C = 4,4'-di-*tert*-butyl-1,1'-biphenyl. (b) Solid-state molecular structure of **1**, **3** and **5** (ellipsoids drawn at the 50% probability level). The hydrogen atoms, except those of the CH$_2$ group, solvent molecules and perchlorate anions are omitted for clarity.

heating. Similarly, elemental forms of chalcogens, including selenium and tellurium powders, remained unreactive.

The ^{31}P{^{1}H} NMR spectra of **3** and **4** are consistent with desymmetrisation of the dppm ligand upon chalcogen insertion. **3** displays two resonances at δ_P = 41.9 and 30.8 ppm (Fig. S9), while **4** shows an AB spin system at 35.4 and 32.8 ppm (Fig. S14). For **3**, the ^1J(P,Se) coupling drops markedly to 484.4 Hz, and the ^{77}Se resonance shifts downfield to δ_{Se} = +70.4 ppm, far from the highly cationic region of [NBu$_4$][Au(C$_3$Se$_5$)$_2$] (≈+988 ppm)[16] and in sharp contrast with free dppmSe.[17]

These results align with our previous IQA calculations on the (^{i}Pr)$_3$P–E series, which showed that selenium exhibits greater charge separation and lower covalent character (70.9%) compared to tellurium (91.2%).[11] In **3**, the electrophilic [(C$_6$F$_5$)$_2$Au]$^+$ fragment withdraws electron density from the P–Se bond, discouraging positive charge build-up at phosphorus and favouring a more delocalised, less polarised P=Se bond.[18] This enhanced delocalisation simultaneously weakens ^1J(P,Se) and produces the observed downfield δ_{Se} shift. Trying to understand the effect the metal can exert, we prepared the phosphonium chalcogenides **5** and **6** by direct methylation of (^{i}Pr)$_3$P=E with MeOTf (Scheme 2). Relative to their Au-bound congeners, the ^{31}P{^{1}H} resonances shift markedly downfield (Fig. S17 and S21), by about +60 ppm for **5** (*vs.* **1** and **2**) and

+35 ppm for **6** (*vs.* **3** and **4**), while the $J_{P,E}$ couplings are slightly smaller than those in the gold(III) complexes. Most strikingly, the $\delta_{Te,Se}$ values move far upfield (Fig. S19 and S23), by more than 250 ppm for **5** and more than 150 ppm for **6**, compared to **1** and **3**, respectively. These trends indicate a different charge distribution: in **5** and **6**, positive charge localises primarily at phosphorus, enhancing the $(^iPr)_3P^+$–E^- resonance form and thereby shielding E and lowering $J_{P,E}$ values. In contrast, the Au(III) complexes **1–4** exhibit an attenuated phosphonium character; the metal withdraws electron density from the chalcogen, yielding a more $(^iPr)_3P$=E-like bond with an electron-depleted E centre. The solid-state structures of **1**, **3** and **5** (Scheme 2b) were confirmed by single-crystal X-ray diffraction.
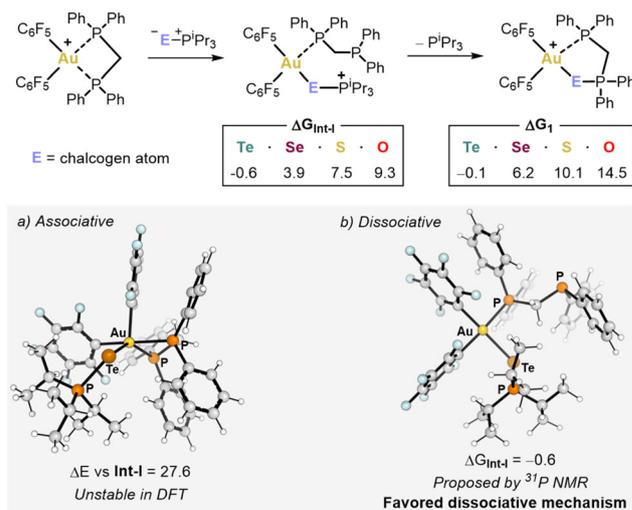
In **1** and **3**, the chalcogen inserts into the Au–P(dppm) bond to give a five-membered Au–E–P–CH$_2$–P metallacycle. The Au(III) centres adopt a nearly ideal square-planar geometry with *cis*-C$_6$F$_5$ groups and a $\kappa^2 E,P$ chelate; key angles fall in the 85.82(6)–93.07(7)° range. For **1**, the Au1–Te1 bond length of 2.5956(4) Å falls within reported Au(III)–Te distances (including bridging Au–Te, 2.61–2.66 Å).[6b] The Au1–P2 bond, 2.3319(6) Å, is slightly shorter than {2.357(2) Å} in [(Ph$_2$PNP(Te)Ph$_2$)Au(μ-Te)]$_2$, indicating a stronger Au–P interaction. The Se analogue **3** is closely related to **1**, with systematically shorter metrics in line with the smaller covalent radius of Se; also, Au1–P2′ remains essentially unchanged (2.3281(5) Å), indicating minimal perturbation of the Au–P bond upon replacing Te with Se. These distances are in line with those observed in other structurally characterised Se–Au–P systems.[19,20] For **5**, the phosphorus atom is tetrahedral; the P1″–Te1″ bond is ≈0.021 Å longer than that in **1**, consistent with the lower $J_{P,Te}$ observed in solution (Scheme 2b). Additionally, in the solid-state structure of **5**, short Te···O contacts between the tellurium centre and the oxygen atoms of the triflate counteranion are clearly observed. Two distinct Te···O interactions are present, with distances of 3.059 Å and 3.451 Å, both shorter than the sum of the van der Waals radii of Te and O (3.58 Å), thus indicating noncovalent chalcogen bonding. Essentially, these interactions arise from two different σ-holes on the same tellurium atom and are oriented *trans* to distinct Te–C/P bonds. The shorter Te···O contact (3.059 Å) lies *trans* to the P1″–Te1′ bond and is associated with a highly directional geometry (P–Te···O = 160.23(3)°), consistent with a stronger σ-hole opposite to the electron-withdrawing phosphonium moiety. In contrast, the longer Te···O interaction (3.451 Å) is oriented *trans* to the Te–Me bond (C1″–Te1′···O = 171.38(5)°) and reflects a weaker σ-hole in this direction due to the donor character of the methyl group. This anisotropic distribution of σ-hole strength highlights the pronounced polarisation of the Te centre in **5**. As a consequence of these directional interactions, each triflate anion bridges two phosphonium telluride cations, and each tellurium atom engages two different oxygen atoms from the triflate anions, giving rise to an extended supramolecular network sustained by bidentate chalcogen bonding (Fig. S26). The observation that a single Te atom simultaneously engages two triflate anions indicates that **5** can

behave as a bidentate ChB donor in the solid state. Such Te···O interactions align with the deep σ-hole predicted later by the ESP analysis and provide a structural snapshot of the type of noncovalent contacts likely involved in substrate activation during chalcogen bond mediated catalysis.

Mechanistic studies on the insertion reaction

We also examined the reactivity trends across the chalcogen series. As E–P(^iPr)$_3$ changes from E = Te to E = O, the stability of both the intermediates and the products decreases (Scheme 3, top). The computed free energies clearly reflect this trend, with tellurium insertion essentially thermoneutral ($\Delta G_1 \approx -0.1$ kcal mol^{-1}) and selenium showing a small but manageable energetic penalty ($\Delta G_1 \approx +6.2$ kcal mol^{-1}), while sulphur and oxygen are less favourable ($\Delta G_1 = +10.1$ and $+14.5$ kcal mol^{-1}, respectively). This periodic dependence is fully consistent with experimental results, where only Te and Se afford isolable products, with selenium requiring thermal activation, and no insertion being observed for the lighter chalcogens. The results highlight the importance of chalcogen polarisability in stabilising the Au–E–P bond, with heavier elements lowering the energetic cost of bond reorganisation and enabling access to viable intermediates and products. To gain further insight into the mechanism underlying this process, we performed theoretical calculations[21,22] to distinguish between two possible approaches for the coordination of phosphane telluride within the Au(III) centre. The first approach involves an associative mechanism, where (^iPr)$_3$PTe would bind to the metal centre before the dissociation of the diphosphane. However, this proved to be unstable in DFT calculations ($\Delta E = 27.6$ kcal mol^{-1} *vs.* **Int-I**), primarily due to high steric crowding between the ^iPr and C$_6$F$_5$ groups (Scheme 3, bottom a).

In contrast, a mechanism involving the prior dissociation of the Au–P bond in [Au(C$_6$F$_5$)$_2$(dppm)]$^+$, creating a free site for the coordination of (^iPr)$_3$PTe and forming **Int-I**, was favoured

	ΔG$_{Int-I}$					ΔG$_1$			
	Te	Se	S	O		Te	Se	S	O
	-0.6	3.9	7.5	9.3		-0.1	6.2	10.1	14.5

E = chalcogen atom

a) Associative

ΔE vs **Int-I** = 27.6
Unstable in DFT

b) Dissociative

ΔG$_{Int-I}$ = −0.6
Proposed by ^{31}P NMR
Favored dissociative mechanism

Scheme 3 DFT mechanistic studies and proposed intermediate. ΔG and ΔE values are shown in kcal mol^{-1}.

with a ΔG of -0.6 kcal mol^{-1} (Scheme 3, bottom b). After the coordination of the diphosphane telluride, the free phosphorus atom of the pendant diphosphane would attack the P–Te bond, extruding P(^{i}Pr)$_3$ and forming a 5-membered cycle. The Au(III) fragment plays a decisive structural and electronic templating role in the chalcogen insertion process. First, coordination of the diphosphane to the square-planar Au(III) centre polarises and weakens the Au–P bond, generating a reactive site that can accommodate the incoming phosphane chalcogenide. Simultaneously, binding of the (^{i}Pr)$_3$P–E fragment to Au(III) increases polarisation of the P–E bond, rendering the chalcogen more susceptible to nucleophilic attack. Beyond this electronic activation, the rigid square-planar geometry of Au(III) enforces a highly organised coordination environment that preorganises the reacting partners. In the case of dppm, the short backbone and constrained bite angle generate a compact chelate that positions the pendant PPh$_2$ arm (**Int-I**) in close proximity to the Au-bound (^{i}Pr)$_3$P–E fragment, thereby lowering the barrier for the intramolecular P–E bond-forming step.

This geometric preorganisation is essential: larger diphosphanes such as dppe (1,2-bis(diphenylphosphane)ethane) or dppBz (1,2-bis(diphenylphosphanyl)benzene) form more flexible and expanded metallacycles that fail to maintain the reactive alignment required for insertion and do not yield chalcogenated products. Thus, Au(III) does not merely act as a Lewis acid, but as a true template that combines electronic activation with enforced spatial organisation, enabling a transformation that is otherwise inaccessible in the absence of metal coordination.

The formation of **Int-I** was further supported by variable temperature ^{31}P{^{1}H} NMR studies (Fig. S24). The formation of complex **1** occurs almost immediately, within less than one minute at -80 °C. At this temperature, a pair of doublets located at $\delta_P = 30.5$ and -2.5 ppm is observed, attributed to the gold-bound phosphorus and tellurated phosphorus atoms, respectively. Upon heating to -60 °C, a new pair of doublets appears, attributed to the monocoordinated diphosphane in **Int-I**, resonating at $\delta_P = 16.9$ and -32.3 ppm. Additionally, a broad singlet is observed around 44.0 ppm, which we attribute to the co-ordinated phosphane telluride in **Int-I**. Furthermore, a pair of signals at $\delta_P = 73.9$ and -23.0 ppm is observed, corresponding to [Au{P(^{i}Pr)$_3$}$_2$]$^+$ and free dppm, respectively, likely due to byproducts derived from the decomposition of **Int-I**. As the sample is heated, the reaction progresses, and the signals of **Int-I** begin to disappear. At room temperature, the signals of complex **1** dominate, although a broad singlet around 40.0 ppm is also observed, which is assigned to unidentified tellurated decomposition side-products. We tentatively attributed the driving force behind tellurium transfer onto the gold(III) complex to the transformation of the constrained 4-membered ring into a 5-membered ring through the addition of the tellurium atom.

ChB catalysis: transfer hydrogenation of 2-phenylquinoline

To further elucidate the origin of the chalcogen-dependent reactivity and catalytic behaviour, we analysed the electrostatic potential (ESP) surfaces of the insertion products **1** and **3**, together with their lighter chalcogen analogues **1-S** and **1-O**, and compared them with the phosphonium chalcogenides **5** and **6** (Scheme 4a).

In all cases, the ESP maps reveal the presence of a σ-hole localised at the chalcogen atom, whose magnitude and spatial definition vary systematically across the chalcogen series. For the Au(III) metallacycles, tellurium-containing complex **1** exhibits the most intense and well-defined σ-hole, with a maximum electrostatic potential ($V_{s,max}$) of 60.4 kcal mol^{-1}, while the selenium analogue **3** shows a slightly reduced but still pronounced σ-hole ($V_{s,max} = 56.2$ kcal mol^{-1}). In contrast, the lighter congeners **1-S** and **1-O** display significantly attenuated σ-hole character, with markedly lower $V_{s,max}$ values, consistent with their diminished polarisability and weaker Lewis acidic behaviour. This progressive decrease in σ-hole strength parallels the calculated thermodynamic trends for chalcogen
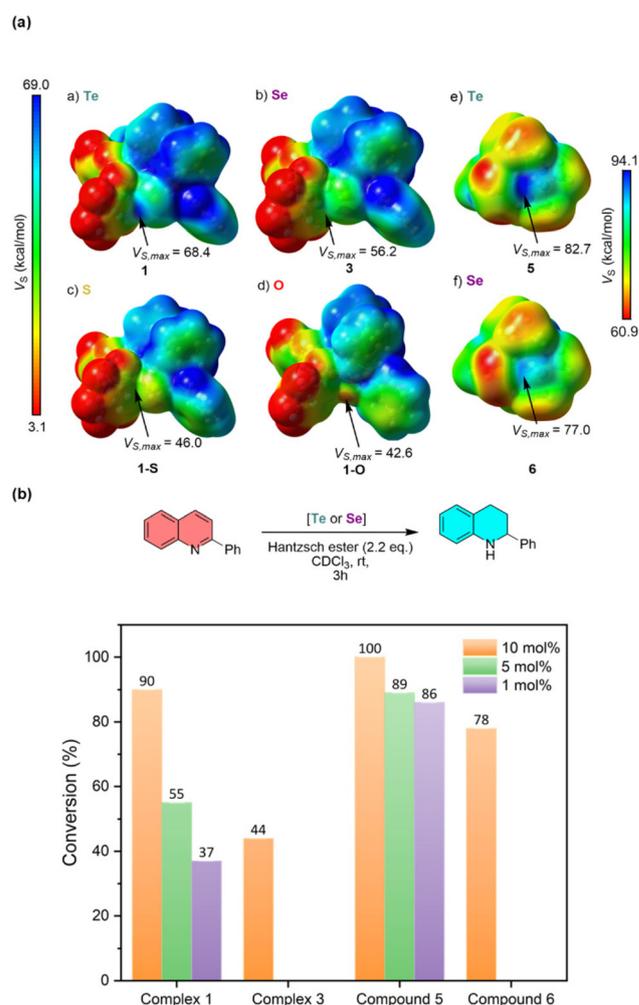
Scheme 4 (a) Electrostatic potential (ESP) surfaces of **1** with different chalcogen atoms and phosphoniums **5**–**6** (in kcal mol^{-1}). The isodensity value is set to 0.0004 e Bohr^{-3}. V_s (kcal mol^{-1}): ESP on the molecular surface. (b) Transfer hydrogenation of 2-phenylquinoline; conversion values are shown in the graph.

insertion and rationalises the experimental observation that only Te and Se afford isolable Au–E–P products.

Phosphonium chalcogenides **5** and **6** also exhibit σ-holes at the chalcogen centre and their electrostatic profiles differ substantially from those of the metallacycles. In particular, **5** displays the highest $V_{s,max}$ value (82.7 kcal mol^{-1}), reflecting strong localisation of positive potential on Te within the phosphonium environment, whereas **6** shows a somewhat reduced σ-hole ($V_{s,max}$ = 77.0 kcal mol^{-1}). Importantly, however, the spatial orientation and accessibility of the σ-hole differ from those in complexes **1** and **3**, underscoring that not only the magnitude but also the geometric presentation of the electrophilic site is crucial for reactivity. Notably, although lower than those typically associated with hypervalent tellurium species, these values are comparable to σ-hole magnitudes reported for Te(IV) tetravalent compounds, such as those described independently by the groups of Mamane and Gabbaï.[23] Coordination to the Au(III) centre significantly modulates the σ-hole at the chalcogen atom. Upon binding, electron density is withdrawn from Se or Te toward the highly electrophilic Au(III) fragment, increasing polarisation of the E–P bond and amplifying the positive electrostatic potential located opposite this bond, the σ-hole responsible for chalcogen-bond donation. In this respect, the Au(III) unit operates in a manner analogous to the phosphonium substituent: both act as strongly electron-withdrawing platforms that intensify the σ-hole magnitude and reinforce chalcogen-bond donor ability, although the metal centre additionally provides geometric constraints and electronic tunability. In this regard, chalcogen-bond (ChB) catalysis exploits the directional σ-hole on Se or Te to engage Lewis-basic sites of a substrate, polarising bonds (*e.g.*, C=N) without Brønsted acidity or redox steps.[24] ChB donor strength increases with chalcogen polarisability and positive charge at E, motivating us to test these donors in ChB catalysis. To directly relate the electronic features extracted from the ESP analysis to catalytic performance, we evaluated all viable chalcogen-containing species in the transfer hydrogenation of 2-phenylquinoline using the Hantzsch ester as the hydride source (Scheme 4b).[23a,25] Among all species examined, the phosphonium chalcogenides **5** and **6** were the most active catalysts.[26] At 10 mol% loading, complex **5** reaches quantitative conversion, while **6** still affords high conversion (78%). Notably, **5** remains highly efficient even at reduced loadings, delivering 89% and 86% conversion at 5 and 1 mol%, respectively, after only 3 hours. To the best of our knowledge, such high efficiency at such low catalyst loadings has not been previously reported for this transformation, underscoring the exceptional ChB donor strength of phosphonium tellurides. These results are fully consistent with the high $V_{s,max}$ values computed for the phosphonium derivatives and confirm their superior ability to activate the substrate through chalcogen bonding.

In comparison, the Au(III) metallacycles exhibit more moderate but still significant catalytic activity. The tellurium-containing complex **1** affords 90% conversion at 10 mol%, decreasing to 55% and 37% at 5 and 1 mol%, respectively. The selenium analogue **3** shows lower activity overall, reaching only 38% conversion at 10 mol%. This diminished reactivity parallels the lower σ-holes observed in the ESP maps of the Au(III) complexes relative to the phosphonium chalcogenides, while preserving the same periodic trend (Te > Se). Control experiments showed that complexes **2** and **4** were not stable under the catalytic conditions, undergoing rapid decomposition accompanied by extrusion of Te or Se, respectively. As a result, although catalytic activity is observed, it cannot be unequivocally attributed to the intact molecular complexes; instead, the active species are likely generated *in situ* from decomposition pathways, potentially involving chalcogen-containing fragments derived from the parent compounds. Importantly, no background reaction is observed in the absence of a catalyst or in the presence of (^{i}Pr)$_3$PTe or (^{i}Pr)$_3$PSe, confirming that all conversion arises from chalcogen-mediated Lewis acid activation.

Conclusions

This work unveils a conceptually new strategy for forging Au–E–P^P (E = Se, Te) complexes through the direct insertion of heavy chalcogens into Au(III)–P bonds, enabling access to tellurated aromatic diphosphanes for the first time. The reaction proceeds under mild conditions and follows a dissociative mechanism, highlighting the ability of gold(III) to mediate main-group element transfer and extend metal–ligand bond activation to the heaviest chalcogens. DFT calculations rationalise the experimental selectivity across the chalcogen series, identifying Te and Se as uniquely capable of stabilising the Au–E–P motif, while S and O are energetically disfavoured. Catalytic studies further show that these insertion products function as Lewis acid catalysts *via* chalcogen bonding. Beyond structural novelty, the catalytic studies reveal distinct and complementary activation modes. Phosphonium chalcogenides, particularly the tellurium derivative, display outstanding Lewis acidity, achieving near-quantitative conversion at catalyst loadings as low as 1 mol% within short reaction times, an efficiency that is unprecedented for this transformation. In comparison, the Au(III) metallacycles exhibit attenuated but still functionally relevant chalcogen activation, offering a modular platform for chalcogen-bond-driven catalysis. Altogether, these results demonstrate that both cationic activation and metal coordination can be exploited to control chalcogen-centred reactivity. This Au-guided chalcogen insertion thus opens new avenues for the design of redox-active diphosphanes, tuneable noncovalent catalysts, and hybrid molecular platforms bridging main-group and transition-metal chemistry.

Author contributions

J. C. P.-S. carried out experimental work, including the synthesis and characterisation of the complexes, as well as the

reactivity studies and catalytic investigations. J. M. and J. V. A.-R. conducted computational studies related to ESP surfaces and mechanisms. M. C. G. and R. P. H. conceptualised the project, supervised the overall work, and wrote the manuscript with the participation of all authors.

Conflicts of interest

There are no conflicts to declare.

Data availability

Supplementary information (SI): detailed data concerning experimental procedures, syntheses, NMR data and computational studies. See DOI: **https://doi.org/10.1039/d6qi00117c**.

CCDC 2522544–2522546 (**1**, **3** and **5**) contain the supplementary crystallographic data for this paper.[27a–c]

Acknowledgements

References

1 (a) K. J. Cavell, Recent fundamental studies on migratory insertion into metal-carbon bonds, *Coord. Chem. Rev.*, 1996, **155**, 209–243; (b) R. Blieck, M. Taillefer and F. Monnier, Metal-catalyzed intermolecular hydrofunctionalization of allenes: easy access to allylic structures via the selective formation of C–N, C–C, and C–O bonds, *Chem. Rev.*, 2020, **120**, 13545–13598; (c) J. Chen, W.-T. Wei, Z. Li and Z. Lu, Metal-catalyzed Markovnikov-type selective hydrofunctionalization of terminal alkynes, *Chem. Soc. Rev.*, 2024, **53**, 7566–7589.

2 (a) E. Kuhlmann, Carbon monoxide insertion into transition metal-carbon sigma-bonds, *Coord. Chem. Rev.*, 1980, **33**, 195–225; (b) T. Bai, S. Ma and G. Jia, Insertion reactions of allenes with transition metal complexes, *Coord. Chem. Rev.*, 2009, **253**, 423–448; (c) B. D. Bergstrom, L. A. Nickerson, J. T. Shaw and L. W. Souza, Transition metal catalyzed insertion reactions with donor/donor carbenes, *Angew. Chem. Int. Ed.*, 2021, **60**, 6864–6878.

3 (a) S. Sahoo, S. M. Mobin and S. Ghosh, Direct insertion of sulfur, selenium and tellurium atoms into metallaborane cages using chalcogen powders, *J. Organomet. Chem.*, 2010, **695**, 945–949; (b) S. Liu, M. Légaré, D. Auerhammer, A. Hofmann and H. Braunschweig, The First Boron–Tellurium Double Bond: Direct Insertion of Heavy Chalcogens into a Mn=B Double Bond, *Angew. Chem., Int. Ed.*, 2017, **56**, 15760–15763; (c) T. Bischof, N. Wieprecht, S. Fuchs, L. Endres, I. Krummenacher, M. Michel, C. Mihm, H. Braunschweig and M. Finze, Unlocking Heteroaromatic Ring Systems through Chalcogen Insertion into Boroles, *Inorg. Chem.*, 2023, **62**, 21329–21335; (d) X. He, Y. Fu, R. Xi, C. Zhang, K. Lan, Z. Su, F. Wang, X. Feng and X. Liu, Asymmetric Carbene Insertion into Se–S Bonds by Synergistic Rh(II)/Guanidine Catalysis Involving Chalcogen–Bond Assistance, *Angew. Chem., Int. Ed.*, 2025, **64**, e202417636; (e) C. Hu, Á. García-Romero, D. Ray, M. Pink and J. M. Goicoechea, Synthesis, Isolation, and Reactivity of a Phosphinidene Telluride, *Angew. Chem., Int. Ed.*, 2025, **64**, e202516494.

4 (a) M. C. Gimeno, in *Handbook of Chalcogen Chemistry New Perspectives in Sulfur, Selenium and Tellurium*, ed. F. Devillanova and W. W. Du Mont, Royal Society of Chemistry, Cambridge, 2007, vol. 2, pp. 37–94; (b) *Organophosphorus Chemistry*, ed. L. J. Higham, D. W. Allen and J. C. Tebby, Royal Society of Chemistry, Cambridge, 2022; (c) A. Nordheider, J. D. Woollins and T. Chivers, Organophosphorus–tellurium chemistry: from fundamentals to applications, *Chem. Rev.*, 2015, **115**, 10378–10406.

5 (a) L. Jeremias, M. Babiak, V. Kubát, M. J. Calhorda, Z. Trávníček and J. Novosad, Successful oxidation of $Ph_2P(CH_2)nPPh_2$ (n = 2, 4, 6) by tellurium leading to $Ph_2P(Te)(CH_2)nP(Te)Ph_2$, *RSC Adv.*, 2014, **4**, 15428–15430; (b) L. Jeremias, M. Babiak, V. Kubát, M. J. Calhorda, Z. Trávníček and J. Novosad, Reaction of $Ph_2P(CH_2)_nPPh_2$ (n = 1, 3, 5) with elemental tellurium and comparison with members of even-numbered series, *Inorg. Chim. Acta*, 2016, **443**, 230–234.

6 (a) M. C. Copsey and T. Chivers, Formation of Ga_2Te_2 and M_3Te_3 (M = Ga, In) rings from reactions of sodium ditelluroimidodiphosphinate with Group 13 halides, *Chem. Commun.*, 2005, 4938–4940; (b) D. J. Eisler, S. D. Robertson and T. Chivers, Gold complexes of ditelluridoimidodiphosphinate ligands—Reversible oxidation of Au(I) to Au(III) via insertion of gold into a phosphorus–tellurium bond, *Can. J. Chem.*, 2009, **87**, 39–46.

7 J. Konu, H. M. Tuononen and T. Chivers, Structural and Spectroscopic Studies of the PCP-Bridged Heavy Chalcogen-Centered Monoanions $[HC(PPh_2E)(PPh_2)]^-$ (E = Se, Te) and $[HC(PR_2E)_2]^-$ (E = Se, Te, R = Ph; E = Se, R = iPr): Homoleptic Group 12 Complexes and One-Electron Oxidation of $[HC(PR_2Se)_2]^-$, *Inorg. Chem.*, 2009, **48**, 11788–11798.

8 (a) M. Lusser and P. Peringer, $[Hg(EPPh_2CHPPh_2)_2]$ (E = S, Se, Te): Organomercury compounds without mercury-

carbon bonds, *Inorg. Chim. Acta*, 1987, **127**, 151–152; (*b*) J. S. Ritch and T. Chivers, Group 11 Complexes of the P, Te-Centered Ligand [TeP^i,P$_2$NP^{i}Pr$_2$]$^-$: Synthesis, Structures, and Insertion Reactions of the Copper(I) Complex with Chalcogens, *Inorg. Chem.*, 2009, **48**, 3857–3865.

9 (*a*) G. Keglevich, Phosphine Chalcogenides, in *Organophosphorus Chemistry*, ed. D. W. Allen, D. Loakes and J. C. Tebby, The Royal Society of Chemistry, 2013, pp. 49–80; (*b*) P. J. W. Elder, T. Chivers and R. Thirumoorthi, Experimental and Computational Investigations of Tautomerism and Fluxionality in PCP- and PNP-Bridged Heavy Chalcogenides, *Eur. J. Inorg. Chem.*, 2013, **2013**, 2867–2876.

10 (*a*) M. C. Copsey, A. Panneerselvam, M. Afzaal, T. Chivers and P. O'Brien, Syntheses, X-ray structures and AACVD studies of group 11 ditelluroimidodiphosphinate complexes, *Dalton Trans.*, 2007, 1528–1538; (*b*) C. Daniliuc, C. Druckenbrodt, C. G. Hrib, F. Ruthe, A. Blaschette, P. G. Jones and W. W. Du Mont, The first trialkylphosphane telluride complexes of Ag(I): molecular, ionic and supramolecular structural alternatives, *Chem. Commun.*, 2007, 2060–2062; (*c*) A. Nordheider, A. M. Z. Slawin, J. D. Woollins and T. Chivers, A silver(I) iodide complex of a tellurophosphorane, *Z. Anorg. Allg. Chem.*, 2015, **641**, 405–407; (*d*) J. C. Pérez-Sánchez, C. Ceamanos, R. P. Herrera and M. C. Gimeno, Unravelling the role of triisopropylphosphane telluride in Ag(I) complexes, *Inorg. Chem. Front.*, 2023, **10**, 6519–6525.

11 J. C. Pérez-Sánchez, C. Ceamanos, J. Echeverría, J. V. Alegre-Requena, R. P. Herrera and M. C. Gimeno, Isolation of elusive gold-phosphane tellurides: From bonding to σ-hole dynamics, *Cell Rep. Phys. Sci.*, 2025, **6**, 102717.

12 (*a*) R. Usón, A. Laguna, M. Laguna, E. Fernandez and M. D. Villacampa, Mono-, bi-, and tri-nuclear bis(diphenylphosphino)methane gold complexes. Crystal and molecular structures of [bis(diphenylphosphino)methane]bis(pentafluorophenyl)gold(III) perchlorate and 1,2; 2,3-di-μ-[bis(diphenylphosphino)methane]-1,3-dichlorotrigold(I) chlorotris(pentafluorophenyl)aurate(III), *J. Chem. Soc., Dalton Trans.*, 1983, 1679–1685; (*b*) R. Usón, A. Laguna, M. Laguna and B. R. Manzano, Synthesis of polynuclear complexes containing the tridentate bis(diphenylphosphino)methanide ligand. Crystal structures of the compounds [(C$_6$F$_5$)$_2$Au(Ph$_2$PCHPPh$_2$)Au(C$_6$F$_5$)] and [(C$_6$F$_5$)$_2$Au(Ph$_2$PCHPPh$_2$)Au(Ph$_2$PCHPPh$_2$)Au(C$_6$F$_5$)$_2$]ClO$_4$, *J. Chem. Soc., Dalton Trans.*, 1984, 839–843; (*c*) R. Usón, A. Laguna, M. Laguna and B. R. Manzano, Synthesis of trinuclear gold(I) and gold(III) complexes containing the tridentate bis(diphenylphosphino)methanide ligand. Crystal structure of [Cl(C$_6$F$_5$)$_2$Au{Ph$_2$PCH(AuNC$_5$H$_5$)PPh$_2$}AuCl], *J. Chem. Soc., Dalton Trans.*, 1985, 2417–2420; (*d*) E. J. Fernandez, M. C. Gimeno, P. G. Jones, A. Laguna, M. Laguna and J. M. López-de-Luzuriaga, Synthesis and structural characterization of polynuclear complexes containing the eight-electron donor bis (diphenylphosphino) metha-

nediide ligand, *J. Chem. Soc., Dalton Trans.*, 1992, 3365–3370.

13 J. Yang, V. Giuso, M.-C. Hou, E. Remadna, J. Forté, H.-C. Su, C. Gourlaouen, M. Mauro and B. Bertrand, Biphenyl Au(III) complexes with phosphine ancillary ligands: synthesis, optical properties, and electroluminescence in Light-Emitting electrochemical cells, *Inorg. Chem.*, 2023, **62**, 4903–4921.

14 L. Rocchigiani, J. Fernandez-Cestau, G. Agonigi, I. Chambrier, P. H. M. Budzelaar and M. Bochmann, Gold (III) Alkyne Complexes: Bonding and Reaction Pathways, *Angew. Chem., Int. Ed.*, 2017, **56**, 13861–13865.

15 T. Chivers and R. S. Laitinen, Tellurium: a maverick among the chalcogens, *Chem. Soc. Rev.*, 2015, **44**, 1725–1739.

16 A. Molter and F. Mohr, Gold complexes containing organoselenium and organotellurium ligands, *Coord. Chem. Rev.*, 2010, **254**, 19–45.

17 J. W. Faller, T. Friss and J. Parr, Hemilability and regioselectivity in palladium and platinum complexes of dppm (E)[E = O, S, Se] ligands, *J. Organomet. Chem.*, 2010, **695**, 2644–2650.

18 S. R. Alvarado, I. A. Shortt, H.-J. Fan and J. Vela, Assessing phosphine–chalcogen bond energetics from calculations, *Organometallics*, 2015, **34**, 4023–4031.

19 C. Taouss and P. G. Jones, Phosphane chalcogenides and their metal complexes. IV. Halogenation products of gold(I) halide complexes of some diphosphane monochalcogenides, *Z. Naturforsch., B: J. Chem. Sci.*, 2016, **71**, 249–265.

20 S. Canales, O. Crespo, M. C. Gimeno, P. G. Jones and A. Laguna, Group 11 Complexes with the Bidentate (SePPh$_2$)$_2$CH$_2$ and Tridentate [(SePPh$_2$)$_2$CH]$^-$ Ligands, *Z. Naturforsch., B: J. Chem. Sci.*, 2007, **62**, 407–412.

21 M. J. Frisch, G. W. Trucks, H. B. Schlegel, *et al.*, *Gaussian 16, Revision C.01*, Gaussian, Inc., Wallingford CT, 2016.

22 AQME 1.5.2; J. V. Alegre-Requena, S. S. V. Sowndarya, R. Pérez-Soto, T. M. Alturaifi and R. S. Paton, AQME: Automated quantum mechanical environments for researchers and educators, *Wiley Interdiscip. Rev.: Comput. Mol. Sci.*, 2023, **13**, e1663.

23 (*a*) B. Zhou and F. P. Gabbaï, AQME: Automated quantum mechanical environments for researchers and educators, *Organometallics*, 2021, **40**, 2371–2374; (*b*) R. Weiss, E. Aubert, P. Pale and V. Mamane, Chalcogen–bonding catalysis with telluronium cations, *Angew. Chem., Int. Ed.*, 2021, **60**, 19281–19286.

24 (*a*) G. Gao, D. Xie and P. Zhou, Chalcogen Bonding Catalysis in Organic Synthesis, *Asian J. Org. Chem.*, 2025, **14**, e202500098; (*b*) C. Zhao, D. Chen, Z. Wang and Y. Zeng, Chalcogen bond in organocatalysis: bonding characteristics, catalytic mechanisms, and catalyst design, *Coord. Chem. Rev.*, 2026, **549**, 217269.

25 (*a*) S. Benz, J. López-Andarias, J. Mareda, N. Sakai and S. Matile, Catalysis with chalcogen bonds, *Angew. Chem., Int. Ed.*, 2017, **56**, 812–815; (*b*) P. Wonner, T. Steinke and S. M. Huber, Activation of quinolines by cationic chalcogen bond donors, *Synlett*, 2019, 1673–1678;

(*c*) R. Weiss, E. Aubert, P. Peluso, S. Cossu, P. Pale and V. Mamane, Chiral chalcogen bond donors based on the 4, 4′-bipyridine scaffold, *Molecules*, 2019, **24**, 4484; (*d*) K. Okuno, R. Nishiyori and S. Shirakawa, Catalysis by tertiary chalcogenonium salts, *Tetrahedron Chem*, 2023, **6**, 100037; (*e*) L. T. Maltz and F. P. Gabbaï, Exploring the Effects of Se Basicity on a Te⋯Se Interaction Supported by a Rigid Indazolium Backbone, *Organometallics*, 2024, **43**, 1246–1255; (*f*) D. Chen, C. Zhao, B. Lu and Y. Zeng, Tetravalent Tellurium–Based Chalcogen Bond Catalysis in the Transfer Hydrogenation of Quinoline: A Theoretical Study, *ChemPhysChem*, 2025, e202500747.

26 Z. Zhao and Y. Wang, Chalcogen bonding catalysis with phosphonium chalcogenide (PCH), *Acc. Chem. Res.*, 2023, **56**, 608–621.

27 (*a*) CCDC 2522544: Experimental Crystal Structure Determination, 2026, DOI: **10.5517/ccdc.csd.cc2qnxdq**; (*b*) CCDC 2522545: Experimental Crystal Structure Determination, 2026, DOI: **10.5517/ccdc.csd.cc2qnxfr**; (*c*) CCDC 2522546: Experimental Crystal Structure Determination, 2026, DOI: **10.5517/ccdc.csd.cc2qnxgs**.